Local trigonal modes and the suppression of the charge density wave in TiSe$_{2-x}$Te$_x$

A. Wegner[*] and D. Louca

Department of Physics, University of Virginia, Charlottesville, Virginia 22904, USA

J. Yang

Department of Physics, Central Michigan University, Mount Pleasant, Michigan 48859, USA

The composition dependence of the charge density wave (CDW) state is investigated in a solid solution of 1T-TiSe$_{2-x}$Te$_2$ using neutron scattering and a pair density function analysis. It is observed that the CDW order is quickly suppressed with doping, between $0.2 \leqslant x \leqslant 0.25$. The suppression of the CDW is coupled with a change in the local symmetry from hexagonal to monoclinic. In the monoclinic, high-temperature phase, a Jahn-Teller (JT) distortion is observed between Ti and Se bonds that is suppressed with Te doping. These observations favor a CDW that is driven by a cooperative JT effect, as Ti-Se bond shortening is crucial to CDW formation and excess chalcogen to Ti charge transfer inhibits the JT mechanism.

I. INTRODUCTION

Transition metal dichalcogenides (TMDs) are quasi-two-dimensional layered materials that exhibit many interesting electronic properties from topological Weyl semimetals [1] to quantum spin liquids [2]. A notable property common to many TMD materials is the charge density wave (CDW) ordering. CDWs frequently occur in proximity to other interesting phenomena, such as superconductivity, in materials with competing order. TMDs such as TiSe$_2$ exhibit prototypical CDW transitions that allow the CDW transition to be studied decoupled from other phenomena. CDWs occur in many polytypes, such as the octohedral 1T and trigonal prismatic 2H, in which the number refers to the number of monolayers in the unit cell and the letter refers to the local coordination of the transition metal atom. 1T-TiSe$_2$ has been extensively studied for its CDW transition occurring upon cooling below 200 K [3]. The mechanism driving this transition is still controversial despite years of research, with exciton condensation [4] and a pseudo–Jahn Teller (JT) effect [5] proposed as candidate processes driving the CDW order. The layered structure makes 1T-TiSe$_2$ a good candidate for thin-film applications [6–9]. Furthermore, superconductivity has been discovered at CDW domain walls under pressure [10], with the intercalation of Cu [11] or substitution of Ti with Ta or Pd [12,13], More recently, TiSe$_2$ has been proposed as a cathode material for Mg ion batteries [14], spurring an increase in interest in the CDW order and revitalizing the effort to understand this phase transition [15–18]. Using a combination of angle-resolved photoemission spectroscopy and neutron scattering on pristine TiSe$_2$, we proposed that a JT mechanism associated with local symmetry breaking in the low-temperature phase is necessary to describe the CDW [19].

On the other end of the phase diagram, TiTe$_2$ does not exhibit a CDW transition for reasons that have not been explored. How the CDW disappears as a function of x in TiSe$_{2-x}$Te$_x$ has not been investigated. While it is to be expected that Te doping will eventually suppress the CDW transition, a study of the solid solution with doping can provide insight into what happens to the lattice with doping. Understanding how the lattice changes between the CDW-forming members in the doping series and the non-CDW-forming members is important to uncovering the lattice effects of CDW formation.

Both 1T-TiSe$_2$ and TiTe$_2$ crystallize in the CdI$_2$-type structure. The structure consists of a hexagonal lattice of Ti atoms surrounded by chalcogen atoms in a trigonally distorted octahedral environment [Fig. 1(a)]. The TiX_6 (X = Se, Te) octahedra are arranged in X-Ti-X layers that are held together by van der Waals forces [20]. The CDW phase of the 1T-TiSe$_2$ is a triple-q state formed by wave vectors $\vec{q}_1 = (\frac{1}{2}, 0, \frac{1}{2})$, $\vec{q}_2 = (0, \frac{\bar{1}}{2}, \frac{1}{2})$, and $\vec{q}_3 = (\frac{\bar{1}}{2}, \frac{1}{2}, \frac{1}{2})$. The electronic character of TiSe$_2$ is a semimetal with a negligible gap, with a hole pocket from the Se 4p band at the Γ point of the Brillouin zone and electron pockets from the Ti 3d bands at M [21]. TiTe$_2$ is a semimetal with an indirect gap of 0.6 eV between the Te 5p and the Ti 3d bands [22]. In this paper we present results from neutron scattering experiments of solid solutions of TiSe$_{2-x}$Te$_x$ showing that the CDW transition is suppressed between $0.2 \leqslant x \leqslant 0.25$, Using pair density function (PDF) analysis we observe changes in the local structure that persist above the CDW transition temperature (T_{CDW}), with atomic distortions indicative of a JT distortion, and we present a phase diagram showing that the CDW transition vanishes between $0.2 \leqslant x \leqslant 0.25$ as Te is doped into TiSe$_2$. We also observe how the trigonal distortions associated with the CDW phase are suppressed with Te doping. It is suggested that Te doping inhibits a cooperative JT effect, which suppresses the CDW phase.
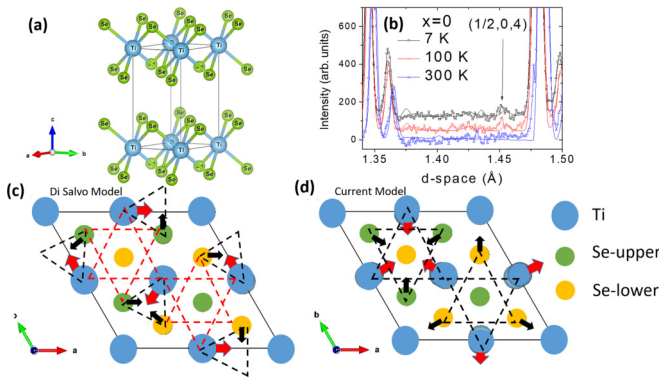
*amw3uv@virginia.edu

FIG. 1. (a) Unit cell for the undistorted hexagonal phase at a high temperature. (b) A temperature-dependent superlattice peak appears below T_{CDW} in the TiSe$_2$ sample. A comparison of (c) the rotation mode distortions that have been previously reported and (d) the breathing mode unit cell consistent with the local structure.

II. EXPERIMENT

Powder samples were prepared by the solid-state reaction method by mixing elemental Ti, Se, and Te. The powders were pelletized and sealed in a quartz tube, heated to $800\,°C$ for 48 h, and slowly cooled to room temperature. They were ground and pelletized for a second time before sintering under the same conditions to increase phase homogeneity. Samples of TiSe$_{2-x}$Te$_x$ were prepared for $x = 0$ (pristine TiSe$_2$), 0.025, 0.05, 0.1, 0.2, 0.25, 0.3, 0.5, 1, and 2 (pristine TiTe$_2$). Experiments were conducted using the constant-wavelength difractometers, BT-1 at the NIST Center for Neutron Research (NCNR) and HB-2A at the High Flux Isotope Reactor (HFIR) at Oak Ridge National Laboratory (ORNL). The wavelengths used for the measurements were $\lambda = 1.540\,Å$(Cu 311) at the NCNR and $\lambda = 1.539\,Å$(Ge 115) at the HFIR. Further measurements were carried out at the time-of-flight neutron diffractometer, the Nanoscale Ordered Materials Diffractometer (NOMAD) at the Spallation Neutron Source (SNS) of ORNL. NOMAD is a diffractometer with a large bandwidth of momentum transfer, Q, and provides the total structure function $S(Q)$. The $S(Q)$ was Fourier transformed into real space to provide the PDF [23,24]. The PDF is a real-space representation of the atomic correlations and does not assume any lattice periodicity. For the Fourier transform of these data, we used a maximum Q of $40\,Å^{-1}$.

PDF analysis is a powerful tool for analyzing the local atomic structure and takes diffuse scattering into account. It is obtained after the sample environment and empty vanadium can are subtracted from the $S(Q)$ and the data are normalized by a vanadium rod. The PDF is a function that contains information about the distribution of distances between atoms in the unit cell and is defined as

$$G(r)_{exp} = \frac{2}{\pi} \int_0^{\infty} Q[S(Q) - 1] \sin(Qr) dQ.$$

A model $G(r)$ can be calculated from the atomic coordinates and unit cell dimensions of the crystal model to obtain

$$G(r)_{mod} = \frac{1}{r} \sum_i \sum_j \frac{b_i b_j}{\langle b \rangle^2} \delta(r - r_{ij}) - 4\pi \rho_0,$$

where b_i is the scattering length for atom i and ρ_o is the atomic density of the crystal. The model $G(r)_{mod}$ is refined to fit the experimental $G(r)_{exp}$ when differences are observed.

III. AVERAGE STRUCTURE

We first begin by describing the average structure. In Fig. 1(b), the diffraction pattern is shown as a function of the temperature for the $x = 0$ system. Earlier studies reported the high-temperature phase of $x = 0$ to be hexagonal with space group $P\bar{3}m1$ and lattice constants $a = b = 3.537 \pm 0.003\,Å$ and $c = 6.00 \pm 0.030\,Å$ [25]. Below 200 K, the CDW state forms and a $2 \times 2 \times 2$ superlattice peak appears while the symmetry changes to $P\bar{3}c1$. The reported crystal structure modulation that leads to the CDW is the one of Di Salvo *et al.* [3], which consists of a rotational distortion and displacements of 0.014 ± 0.003 and $0.042 \pm 0.007\,Å$ of the Se and Ti atoms, respectively, around the Star of David motif. Given that the Te distortion is larger than the Se distortion the Star of David becomes distorted. The result of the distortion is the creation of TiSe$_2$ trimers with slightly shortened bonds [3] as shown in Fig. 1(c).

Superlattice peaks at half-integer (hkl) indices of the primitive hexagonal unit cell are observed [Fig. 1(b)]. The CDW distortion is small, thus the intensity of the CDW peaks are of the order of 1% of the non-CDW peaks, which is comparable to the intensity of the reflections reported from single-crystal diffraction [3]. The superlattice peaks are similar in intensity to the peaks arising from impurities such as elemental Ti, Se, and Te, hence a superlattice reflection is shown with a 2θ that does not coincide with reflections from the extra phases. Figure 1(b) shows the temperature dependence of the $(\frac{1}{2}, 0, 4)$ peak in TiSe$_2$. The diffraction data are fit using the reported symmetries of $P\bar{3}c1$ at 7 and 100 K and $P\bar{3}m1$ at 300 K with $\chi^2 = 3.57$, 3.49, and 4.43, respectively.

Upon doping, the low-temperature symmetry remains unchanged but the CDW transition is quickly suppressed. Shown in Fig. 2(a) is a plot of the diffraction patterns at two temperatures for $x = 0.2$. Evidence of the commensurate CDW order is observed in this composition as well, but by $x = 0.25$, shown in Fig. 2(b), the CDW transition is suppressed.

As x increases as seen in the nominally $x = 1$ sample the low-temperature crystal symmetry deviates from the hexagonal lattice of TiSe$_2$. At low-d spacing shoulders appear on Bragg peaks as shown in the expanded range of the diffraction data in Fig. 2(c) that are indicative of a monoclinic distortion. The diffraction patterns for $x = 1$ can be fit using the symmetry $P2/m$ with $\chi^2 = 4.881$. Refinement of occupancy of Se and Te suggests that the stoichiometry is closer to $x = 0.6$, although the unit cell size agrees with the literature [26]. No CDW is observed and the material does not show a structural phase transition upon warming. At $x = 2$, in TiTe$_2$, no CDW peaks are observed either [Fig. 2(d)], consistent with the average structure reported in previous studies of TiTe$_2$.

IV. LOCAL STRUCTURE

The observed CDW peaks cannot be uniquely described by the $P\bar{3}c1$ symmetry, however. As we recently found, a superlattice with identical lattice constants and distortions
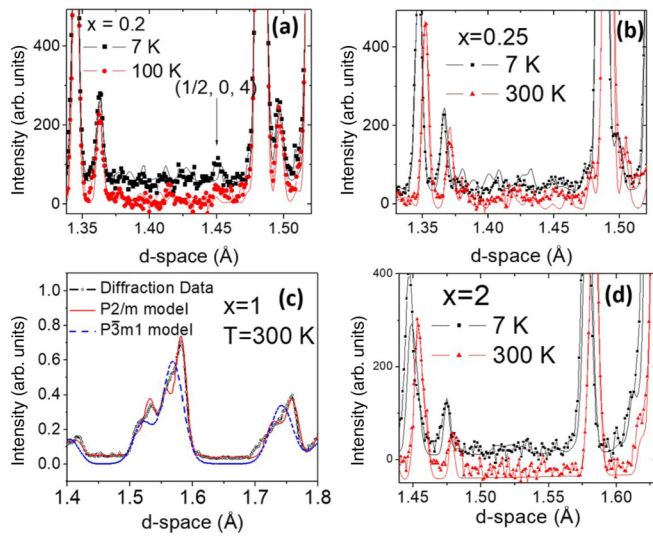
FIG. 2. (a) As Te is doped into the system the superlattice peak still appears at $x = 0.2$. (b) At $x = 0.25$ the superlattice peak is no longer present and the CDW has been suppressed. (c) At $x = 1$ shoulders appear on peaks in the diffraction pattern due to the monoclinic local structure. (d) The superlattice peak does not appear at the Te end of the doping spectrum.

FIG. 3. (a) The local structure of TiSe$_2$ in the low-temperature CDW phase is fit with the previously reported $P\bar{3}c1$ model and with a $P\bar{3}m1$ model. Both fit long-range correlations well but only the $P\bar{3}m1$ model can reproduce splitting of the first peak. (b) The high-temperature-phase local structure is fit with the hexagonal average structure and with a monoclinic model. Only the monoclinic model can reproduce correlations above 9 Å.

described using $P\bar{3}m1$ symmetry fits the average structure of TiSe$_2$ as well, while improving the fit of the local distortions [19]. The $P\bar{3}m1$ symmetry contains a breathing-mode distortion, while the $P\bar{3}c1$ symmetry contains a rotational distortion. Local analysis must be employed to see how the distortions occur in the solid solution. Shown in Fig. 2 is the $G(r)$ corresponding to the local atomic structure of TiSe$_2$ at 2 K [Fig. 2(a)] and 300 K [Fig. 2(b)]. The negative Ti-Se correlation peak at 2.55 Å has a shoulder to the left at 2.41 Å. The magnitude of the split is not temperature dependent but the intensity is. This is shown in the insets in Fig. 3. The $P\bar{3}c1$ CDW model of Di Salvo fits the local structure of the 2 K data well except for the first Ti-Se peak. This is shown in Fig. 2(a) and in the inset. While the distortions associated with the CDW phase lead to shortened Se-Ti-Se trimers as shown in Fig. 1(c), the bonds are shortened by only 0.06 Å, which is not nearly enough to reflect the distortion in the local strucutre. However, when the symmetry constraints are relaxed to $P\bar{3}m1$ the first peak can be fit well as shown in the figure. This is because in this symmetry, the constraints of the atom displacements are lifted and the Ti atoms move to form a breathing mode, rather than Ti atoms being constrained to move along the **a** or **b** axis toward another Ti atom as in the $P\bar{3}c1$ symmetry, where **a** and **b** are the lattice vectors of the primitive hexagonal unit cell. With $P\bar{3}m1$ symmetry, Ti atoms move toward Se atoms with a JT-like breathing distortion, shown in Fig. 1(d) in comparison to the Di Salvo model in Fig. 1(a) and it fits the local structure very well. This breathing distortion shortens the bonds of $\frac{1}{8}$ Ti-Se nearest-neighbor bonds, as six of the eight Ti atoms in the unit cell move toward one of their six neighbors. In the non-CDW phase, above 200 K, the distortions are still present. At high temperatures, the long-range correlations of the PDF cannot be fit with the hexagonal symmetry $P\bar{3}m1$ despite the good fit of the
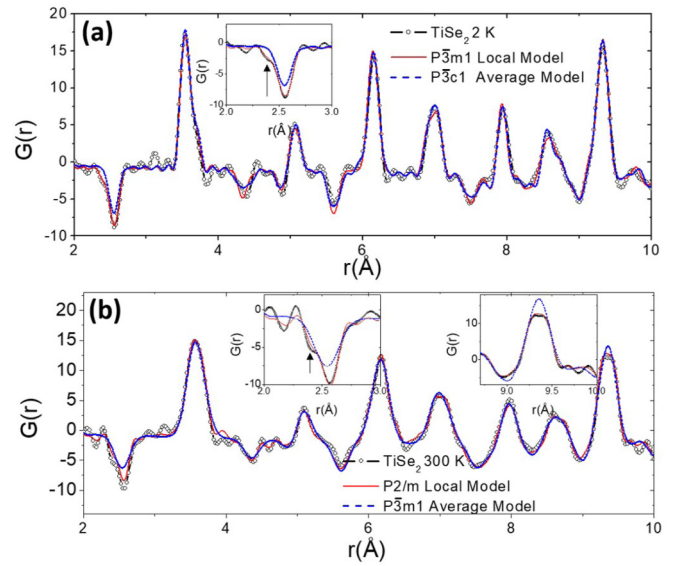
average structure using this symmetry. A local monoclinic model improves the fit as shown in Fig. 3(b). At long distances of $r > 9$ Å above T_{CDW}, peaks corresponding to correlations two unit cells away split into separate distinct peaks [see inset in Fig. 3(b)].

At $x = 0.1$, the splitting of the first Ti-Se peak is unchanged, as shown in Figs. 4(a) and 4(b). The peak at 2.55 Å has a shoulder at 2.41 Å for $x \leqslant 0.1$. The concentration of Te is too low to observe a separate Ti-Te pair correlation. At high temperatures the peak is more apparent because the shoulder peak is sharper while the main peak becomes broader. At correlations larger than 9 Å, there is a significant change above the T_{CDW}. Most notably, the peak at 9.34 Å [Fig. 4(c)] splits into two. This splitting can be fit using a monoclinic symmetry with space group $P2/m$. The temperature at which this splitting occurs decreases as the concentration of Te is increased. This peak is primarily composed of Se-Se correlations. The correlations are made up of Se atoms that are separated by a translation of $2\mathbf{a} - \mathbf{b}$ and all symmetry equivalents. Figure 4(d) shows two of the correlations that split due to the high-temperature monoclinic distortion that breaks the $a = b$ symmetry.

The $G(r)$ of the $x = 1$ sample fits the monoclinic phase, with $a = 25.004 \pm 0.011$ Å, $b = 11.0072 \pm 0.0041$ Å, $c = 12.6097 \pm 0.0071$ Å, $\beta = 88.752 \pm 0.057$ observed in the average structure. As the Se and Te atoms are different sizes, separate peaks occur at 2.55 and 2.79 Å, corresponding to Ti-Se and Ti-Te nearest-neighbor peaks, respectively. Integration of the peaks at 2.55 and 2.79 Å suggests that the stoichiometry of the sample is closer to $x = 0.65$. The peaks at 2.55 and 2.79 Å are symmetric and there is no evidence of the JT distortion observed in the CDW materials. For $x = 2$, there
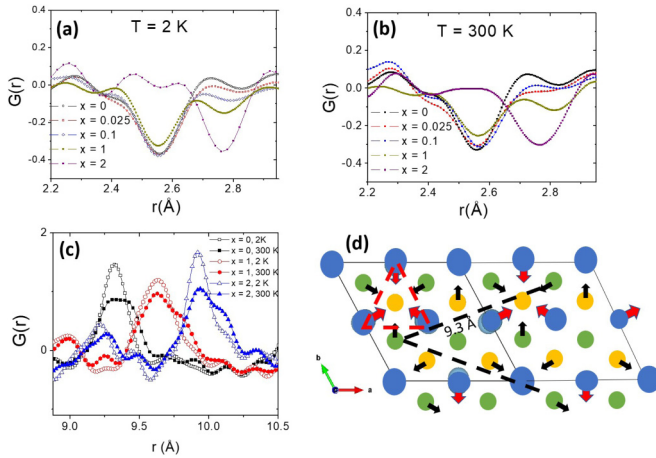
FIG. 4. (a) Composition dependence of the first Ti-Se and Ti-Te peak at 2 K showing that at low concentrations a shoulder appears on the first peak that is not present in the $x = 1$ and $x = 2$ samples. (b) Composition dependence of the first Ti-Se and Ti-Te peak at 300 K shows that the splitting of the first peak occurs even above the T_{CDW}. (c) The PDF above 9 Å shows that at high temperatures the long-distance correlations become split as a monoclinic distortion breaks the $a = b$ axis symmetry. (d) Dashed red lines show the triangles of Ti that shift toward Se to cause the distortion shown in (a) and (b). Dashed black lines indicate correlations of 9.3 Å that, along with symmetry equivalent correlations outside the plotted region, make up the peak shown in (c).

FIG. 5. Phase diagram for the TiSe$_{2-x}$Te$_x$ system. The CDW transition is suppressed with Te doping and does not appear above a Te concentration of 12.5%.

is no splitting of the nearest-neighbor Ti-Te peak at 2.8 Å and no JT distortion is observed in the local structure. As a function of temperature the local trigonal symmetry is broken as in the high-temperature phase of the doping series.

The results indicate that the JT distortion exists above T_{CDW} and becomes cooperative when the CDW forms. This model retains the breathing-mode distortions with the same bond lengths as the CDW phase while breaking the overall local trigonal symmetry.

V. DISCUSSION

The composition dependence of the CDW order is shown in the phase diagram in Fig. 5. It is clear that as Te is doped into the system, the CDW transition is suppressed. For $x = 0.025$, T_{CDW} is between 150 and 190 K. For $x = 0.1$ the transition occurs between 100 and 150 K. From the presence of superlattice peaks, the highest doping level to undergo the CDW transition is $x = 0.2$, while the absence of superlattice reflections in $x = 0.25$ and $x = 0.3$ corresponds to the absence of the CDW order.

Splitting of the first Ti-Se peak associated with a trigonal distortion is clearly observed in the local structure for samples with a CDW phase. This splitting does not occur when the concentration of Te is high enough that the CDW is suppressed. As this splitting occurs even at high temperatures, well above the T_{CDW}, there is a clear connection between the distortions and CDW formation. The magnitude of the Ti-Se distortion and the percentage of bonds distorted remain constant for small x despite a decrease in T_{CDW}. It is likely that competition between disorder introduced by Te and the
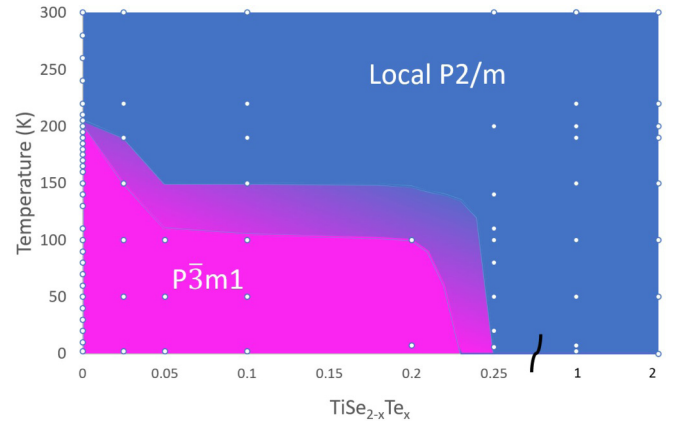
tendency toward a long-range cooperative JT order with Se leads to a lowering of the transition temperature.

As mentioned earlier, the suggested mechanism behind the CDW transition is exciton condensation or a pseudo-JT effect. Exciton formation occurs due to a weakly screened Coulomb interaction between the hole pocket of the Se $4p$ band at Γ and the electron pocket of the Ti $3d$ band at L. In order for the hole and electron pockets to coincide in the Brillouin zone the lattice periodicity must be doubled. Although evidence supports the existence of excitons in the TiSe$_2$ system, the CDW has been observed even when the excitons are suppressed by terahertz pulses [27].

Multiple models that consider a JT mechanism have been proposed for the TiSe$_2$ system. The model proposed by Hughes [5], for instance, suggests that the energy of a partially occupied d_{z^2} band is lower in a trigonal prismatic 2H crystal field than in an octahedral 1T field. In this model, the rotational modes of B-site Se about Ti lead to a configuration intermediate between the 2H and the 1T polytypes.

The d-electron occupancy of TiSe$_2$ is quite small and close to d^0, while the count in TiTe$_2$ is closer to $d^{\frac{1}{3}}$, as the size of Te atoms leads to greater chalcogen–to–transition metal charge transfer [28]. The Hughes model suggests an increase in charge transfer with Te doping initially leading to a more robust CDW. The suppression of the CDW with doping combined with no observation of the rotational modes in the local structure makes the Hughes mechanism unlikely.

The Whangbo [29] model, on the other hand, requires a JT-driven CDW transition to shorten the Ti-Se bond length. This reduces the energy by delocalizing electrons and allows for hybridization between the Ti $3d$ and the Se $4p$ orbitals. In this model, the p band is lowered and the transition does not rely on chalcogen-to-Ti charge transfer.

On the other hand, the Whangbo model can account for the dependence of the transition on Te doping. Consistent with our measurements, the trigonal phase is suppressed when Te is substituted into the lattice. Te disrupts the electronic homogeneity of the crystal and inhibits the cooperative JT observed in pure TiSe$_2$. A possible explanation for this is that Te orbitals are more diffuse [28] and Te atoms are heavier than Se, so the energy gained through orbital overlap is diminished

at the Ti-Te sites. As the Te electrons are more mobile, this may increase charge transfer to Ti d bands, as the reduced p occupancy of the chalcogen sites leads to a weaker interaction.

Further evidence that would support that charge transfer suppresses the CDW comes from the monoclinic distortion above T_{CDW}. It is unusual for a high-temperature phase to have lower symmetry than the low-temperature phase. Despite this, the local structure analysis suggests that there is a monoclinic distortion of the local structure. $CrSe_2$ is a material that undergoes a similar phase transition [30]. $CrSe_2$ has a low-temperature trigonal symmetry ($P\bar{3}m1$) with a monoclinic intermediate-temperature phase ($I2/m$) that is caused by charge transfer to Cr, leading to a degeneracy in the t_{2g} band that breaks the threefold rotation symmetry. In $TiSe_{2-x}Te_x$ this monoclinic distortion breaks up the long-range order associated with the CDW. At low temperatures a cooperative JT effect drives orbital ordering that leads to a CDW phase. As the temperature increases above T_{CDW}, thermal fluctuations could lead to charge transfer on Ti. A degeneracy in the t_{2g} band of Ti can break the local C_3 symmetry while preserving the short-range distortions, as observed in the local structure.

[1] Y. Sun, S.-C. Wu, M. N. Ali, C. Felser, and B. Yan, Phys. Rev. B **92**, 161107(R) (2015).

[2] K. T. Law and P. A. Lee, Proc. Natl. Acad. Sci. USA **114**, 6996 (2017).

[3] F. J. Di Salvo, D. E. Moncton, and J. V. Waszczak, Phys. Rev. B **14**, 4321 (1976).

[4] H. Cercellier, C. Monney, F. Clerc, C. Battaglia, L. Despont, M. G. Garnier, H. Beck, P. Aebi, L. Patthey, H. Berger *et al.*, Phys. Rev. Lett. **99**, 146403 (2007).

[5] H. Hughes, J. Phys. C: Solid State Phys. **10**, L319 (1977).

[6] P. Goli, J. Khan, D. Wickramaratne, R. K. Lake, and A. A. Balandin, Nano Lett. **12**, 5941 (2012).

[7] K. Sugawara, Y. Nakata, R. Shimizu, P. Han, T. Hitosugi, T. Sato, and T. Takahashi, ACS Nano **10**, 1341 (2015).

[8] P. Chen, Y.-H. Chan, X.-Y. Fang, Y. Zhang, M.-Y. Chou, S.-K. Mo, Z. Hussain, A.-V. Fedorov, and T.-C. Chiang, Nat. Commun. **6**, 8943 (2015).

[9] M. Noh, D. C. Johnson, and G. S. Elliott, Chem. Mater. **12**, 2894 (2000).

[10] A. F. Kusmartseva, B. Sipos, H. Berger, L. Forró, and E. Tutiš, Phys. Rev. Lett. **103**, 236401 (2009).

[11] E. Morosan, H. Zandbergen, B. Dennis, J. Bos, Y. Onose, T. Klimczuk, A. Ramirez, N. Ong, and R. Cava, Nat. Phys. **2**, 544 (2006).

[12] H. Luo, W. Xie, J. Tao, I. Pletikosic, T. Valla, G. S. Sahasrabudhe, G. Osterhoudt, E. Sutton, K. S. Burch, E. M. Seibel *et al.*, Chem. Mater. **28**, 1927 (2016).

[13] E. Morosan, K. E. Wagner, L. L. Zhao, Y. Hor, A. J. Williams, J. Tao, Y. Zhu, and R. J. Cava, Phys. Rev. B **81**, 094524 (2010).

[14] Y. Gu, Y. Katsura, T. Yoshino, H. Takagi, and K. Taniguchi, Sci. Rep. **5**, 12486 (2015).

[15] T. E. Kidd, T. Miller, M. Y. Chou, and T.-C. Chiang, Phys. Rev. Lett. **88**, 226402 (2002).

[16] G. Li, W. Z. Hu, D. Qian, D. Hsieh, M. Z. Hasan, E. Morosan, R. J. Cava, and N. L. Wang, Phys. Rev. Lett. **99**, 027404 (2007).

[17] M. Calandra and F. Mauri, Phys. Rev. Lett. **106**, 196406 (2011).

[18] C. Monney, H. Cercellier, F. Clerc, C. Battaglia, E. F. Schwier, C. Didiot, M. G. Garnier, H. Beck, P. Aebi, H. Berger, L. Forró, and L. Patthey, Phys. Rev. B **79**, 045116 (2009).

[19] A. Wegner, J. Zhao, J. Li, J. Yang, A. Anikin, G. Karapetrov, D. Louca, and U. Chatterjee, arXiv:1807.05664.

[20] C. M. Fang, R. A. de Groot, and C. Haas, Phys. Rev. B **56**, 4455 (1997).

[21] T. Rohwer, S. Hellmann, M. Wiesenmayer, C. Sohrt, A. Stange, B. Slomski, A. Carr, Y. Liu, L. M. Avila, M. Kalläne *et al.*, Nature **471**, 490 (2011).

[22] D. K. G. de Boer, C. F. van Bruggen, G. W. Bus, R. Coehoorn, C. Haas, G. A. Sawatzky, H. W. Myron, D. Norman, and H. Padmore, Phys. Rev. B **29**, 6797 (1984).

[23] B. E. Warren, *X-ray Diffraction* (Courier Corp., North Chelmsford, MA, 1990).

[24] P. Peterson, M. Gutmann, T. Proffen, and S. Billinge, J. Appl. Crystallogr. **33**, 1192 (2000).

[25] D. L. Greenaway and R. Nitsche, J. Phys. Chem. Solids **26**, 1445 (1965).

[26] Y. Arnaud and M. Chevreton, J. Solid State Chem. **39**, 230 (1981).

[27] M. Porer, U. Leierseder, J.-M. Ménard, H. Dachraoui, L. Mouchliadis, I. Perakis, U. Heinzmann, J. Demsar, K. Rossnagel, and R. Huber, Nat. Mater. **13**, 857 (2014).

[28] E. Canadell, R. Brec, J. Rouxel, M.-H. Whangbo *et al.*, J. Solid State Chem. **99**, 189 (1992).

[29] M. H. Whangbo and E. Canadell, J. Am. Chem. Soc. **114**, 9587 (1992).

[30] S. Kobayashi, H. Ueda, D. Nishio-Hamane, C. Michioka, and K. Yoshimura, Phys. Rev. B **89**, 054413 (2014).